Random Matrix Theory Applied to Acoustic Backscattering and Imaging In Complex Media

Alexandre Aubry and Arnaud Derode

Laboratoire Ondes et Acoustique, ESPCI, Université Denis Diderot (Paris VII), CNRS (UMR 7587), 10 rue Vauquelin, 75005 Paris, France

(Received 5 September 2008; revised manuscript received 16 January 2009; published 26 February 2009)

The singular values distribution of the propagation operator in a random medium is investigated in a backscattering configuration. Experiments are carried out with pulsed ultrasonic waves around 3 MHz, using an array of transducers. Coherent backscattering and field correlations are taken into account. Interestingly, the distribution of singular values shows a dramatically different behavior in the single and multiple-scattering regimes. Based on a matrix separation of single and multiple-scattered waves, an experimental illustration of imaging through a highly scattering slab is presented.

DOI: 10.1103/PhysRevLett.102.084301 PACS numbers: 43.60.+d, 02.10.Yn, 42.25.Dd, 46.65.+g

When probing an unknown medium with waves (e.g., for imaging or communication purposes) an important issue is the importance of multiple scattering relative to single scattering. Though it gives rise to fascinating phenomena in mesoscopic physics, multiple scattering is a nightmare for classical imaging techniques, which are based on the first Born approximation. In wave physics, a matrix formalism is particularly appropriate when the wave field can be controlled by transmission or reception arrays of N independent elements. Since an inhomogeneous medium can be treated as one realization of a random process, some aspects of random matrix theory (RMT) may be fruitfully applied to imaging. In this Letter, we present experimental results with wide-band ultrasonic waves propagating in complex media, in connection with RMT. This work benefits from previous studies regarding multiple scattering of waves [1], and from RMT [2] in connection with telecommunication [3,4] or scattering [5,6] problems. First, we study the propagation operator (termed $\mathbf{K}$) in a backscattering configuration, where single and multiple scattering coexist. $\mathbf{K}$ is an N by N complex matrix, symmetric (due to reciprocity) but not Hermitian; hence, it belongs to neither the Gaussian orthogonal (GOE) nor to the Gaussian unitary (GUE) ensembles. A singular value decomposition (SVD) consists in writing $\mathbf{K} = \mathbf{U}\mathbf{\Lambda}\mathbf{V}^{\dagger}$, where $\mathbf{U}$ and $\mathbf{V}$ are unitary and $\mathbf{\Lambda}$ is a diagonal matrix whose nonzero elements λ_i are called the singular values of $\mathbf{K}$. They are always real and positive. The distribution of singular values $\rho(\lambda)$ is a relevant observable. We show that, not entirely surprisingly, though we have a limited number of elements ($N = 64$) and a single realization of disorder, $\rho(\lambda)$ is well described by the quarter-circle law [3,7] as long as multiple scattering dominates. Interestingly, this is no longer true when single scattering dominates: a different distribution (Hankel) is observed. Second, we show how matrix properties can be taken advantage of to discriminate single- from multiple-scattered waves and hence improve drastically imaging and detection through a strongly scattering medium. This approach can be applied to all fields of wave physics (e.g., acoustics, microwave, seismology) for which the multielement arrays are available and provide time-resolved measurements of the wave field.

The experimental setup (Fig. 1) uses an ultrasonic array in the 2.5–3.5 MHz bandwidth. Each array element is 0.39 mm in size and the array pitch p is 0.417 mm. The magnitude of the electroacoustic frequency response of each element has been measured, in order to compensate for possible differences in sensitivity. The sampling frequency is 20 MHz. The array is immersed in water, at a distance a from a random scattering medium. N^2 time responses are measured by sending a pulse at element i and recording the scattered wave field at element j, for every possible values of i and j. The resulting signals are truncated into overlapping windows with length δt chosen so that signals associated with the same scattering path within the medium arrive in the same time window, while keeping a satisfying time resolution. A short-time discrete Fourier analysis gives a set of matrices $\mathbf{K}$. A numerical SVD provides N singular values λ_i at each time and frequency. $\mathbf{K}$ is renormalized into $\tilde{\mathbf{K}}$ such that

$$\tilde{\lambda}_i = \lambda_i \Big[\sum_{p=1}^{N} \lambda_p^2 / N \Big]^{-1/2} \tag{1}$$

in order to facilitate the comparison with the dimensionless theoretical predictions of RMT. We form the histogram of

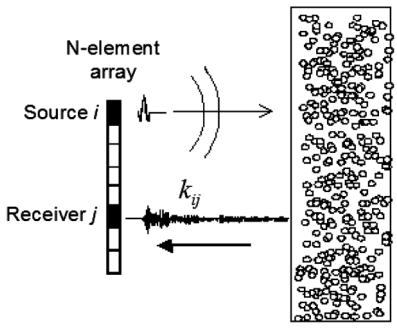

FIG. 1. Experimental setup.

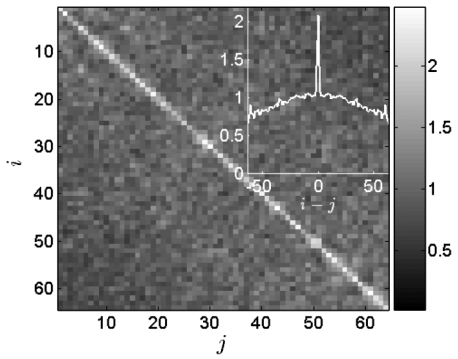

FIG. 2. Mean intensity $I_{ij} = \langle |\tilde{k}_{ij}|^2 \rangle$ of coefficients $\tilde{k}_{ij}$, normalized by $1/N$ and averaged over all times t and frequencies f. The graph on the top right corner represents I_{ij} as a function of i-j.

the whole set of renormalized singular values, taken over every index i, time t and frequency f, and obtain an estimator $\hat{\rho}$.

The first sample we consider is essentially two-dimensional; it is a random collection of parallel steel rods with radius 0.4 mm and concentration 0.12 mm^{-2}. We set $a = 25$ mm and $\delta t = 10$ μs. In the 2.5–3.5 MHz range, the average value of the elastic mean-free path has been obtained by coherent transmission measurements : $l_e = 7.7$ mm [8]. We first consider the multiple-scattering regime ($ct \gg l_e$, where c is the wave speed), setting $t > 35$ μs (the origin of time corresponds to the arrival of the first echo), and compare $\hat{\rho}(\lambda)$ with the quarter-circle law $\rho_{\mathrm{QC}}(\lambda) = \sqrt{4 - \lambda^2}/\pi$ $(0 < \lambda < 2)$ [3,9], which applies for an $N \times N$ matrix ($N \gg 1$) whose complex elements are zero-mean independent and identically distributed (*i.i.d*) variables with variance $1/N$.

Physically, in the multiple-scattering regime the matrix elements cannot be identically distributed: the diagonal elements have a double variance (Fig. 2) due to weak localization. Here the coherent backscattering enhancement [10] is strictly limited to the diagonal elements because the peak width ($a/k\sqrt{Dt}$ with k the wave number, and the diffusion constant $D \sim 4$ mm$^2/\mu$s) is smaller than the array pitch. Since $kl_e \sim 100$, strong localization effects can be ignored [1]. Away from the diagonal, the variance is not constant either but decays slowly due to the progressive growth of the incoherent diffusive halo inside the scattering medium [11]. This nonuniform variance, as well as symmetry of $\mathbf{K}$, can be proved to have an negligible impact on ρ as long as $N \gg 1$.

However, there are also short-range correlations between elements of $\mathbf{K}$. They can be estimated by the correlation coefficient Γ:

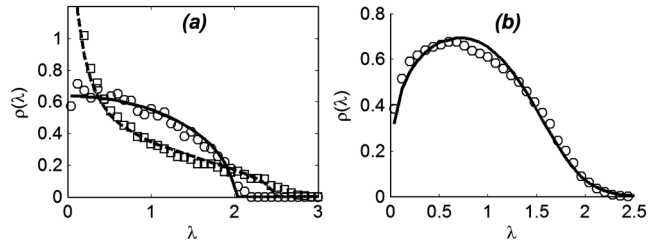

FIG. 3. Distribution of singular values. (a) Multiple-scattering regime: Correlations are either removed (white disks, quarter-circle law: solid line) or taken into account (squares, theory: dashed line). (b) Single-scattering regime: $\hat{\rho}(\lambda)$ (white disks) is compared to $\rho_H(\lambda)$ (continuous line).

$$\Gamma_m = \langle \tilde{k}_{i,j} \tilde{k}^*_{i,j+m} \rangle / \langle |\tilde{k}_{i,j}|^2 \rangle \tag{2}$$

where the symbol $\langle . \rangle$ denotes an average over t, f and couples (i, j). These correlations have two physical origins. First, there is a mechanical coupling between neighboring array elements. Second, the observed wave field has a nonzero coherence length, as stated by the van Cittert-Zernike theorem [12]. In this experiment, the residual correlations are limited to adjacent elements ($\Gamma_{\pm 1} \simeq 0.5$). A solution to get rid of them is to consider only one in two array elements and reduce the matrix size to 32×32. The resulting distribution $\hat{\rho}(\lambda)$ is plotted in Fig. 3(a) and is in reasonable agreement with ρ_{QC}, though N is finite. Another, yet more complicated, way is to incorporate Γ_m in a theoretical model [13]. The resulting theoretical ρ is found in reasonable agreement with the experimental results [Fig. 3(a)]. So it seems that in the multiple-scattering regime, the probability density function for singular values of the backscattering matrix can be fairly well predicted from RMT, even by the simple quarter-circle law in the case where field-field correlations can be removed.

Interestingly, experimental results show that this is no longer true when single-scattering dominates, i.e., at earlier times ($ct < l_e$). An interpretation can be given, under Fresnel's approximation. Without loss of generality, in a 2D configuration the matrix elements read

$$k_{ij}(t, f) \propto \frac{\exp(j2kR)}{R} \sum_{d=1}^{N_d} A_d \exp\left[jk \frac{(x_i - X_d)^2}{2R} \right] \times \exp\left[jk \frac{(x_j - X_d)^2}{2R} \right], \tag{3}$$

where $R = ct/2$, $x_i = (i - N/2)p$ is the coordinate along the array. X_d is the transverse position of the dth scatterer which contributes to the backscattered wave at time t, the amplitude A_d depending on its reflectivity. Both A_d and X_d are considered random. k_{ij} can be rearranged as

$$k_{ij} \propto \underbrace{\frac{\exp(j2kR)}{R} \exp\left[jk \frac{(x_i - x_j)^2}{4R} \right]}_{\text{deterministic term}} \underbrace{\sum_{d=1}^{N_d} A_d \exp\left[jk \frac{(x_i + x_j - 2X_d)^2}{4R} \right]}_{\text{random term}}. \tag{4}$$

The term before the sum in Eq. (4) does not depend on the scatterers distribution, contrary to the term on the right. This implies that whatever the realization of disorder, there is a deterministic phase relation between coefficients of $\mathbf{K}$ located on the same antidiagonal, i.e., for couples of transmitter (i) and receiver (j) such that $i + j$ is constant

$$\beta_m = k_{i-m,i+m}/k_{ii} = \exp[jk(mp)^2/R]. \quad (5)$$

As a consequence, single scattering manifests itself as a particular coherence of the matrix along its antidiagonals (Fig. 4). This is valid independently of the scatterers configuration, without any ensemble averaging, under two conditions: single scattering and Fresnel's approximation. The parabolic phase dependence predicted by Eq. (5) is compared in Fig. 4(b) with the coefficient β_m obtained experimentally.

What is the impact of this particular coherence on $\rho(\lambda)$? A second experiment is carried out with the same device, in a weakly scattering medium (agar-gelatine gel with $l_e \simeq 1000$ mm). This is necessary because in the rods sample, l_e is so small that single scattering dominates only during the first 10 μs at best, which is enough to measure β_m (no averaging is needed), but not enough to have a statistically significant estimation of $\rho(\lambda)$. Here $a = 50$ mm, $\delta t = 10$ μs. Γ_m spreads until $|m| = 2$: the matrices $\mathbf{K}(t, f)$ have been truncated by keeping only one in three elements before computing $\hat{\rho}(\lambda)$.

To our knowledge, this kind of random matrix whose antidiagonal elements are linked with a deterministic phase relation have not been yet investigated theoretically. But their properties are close to those of a random Hankel matrix, i.e., a $N \times N$ random matrix whose antidiagonal elements are equal. We have checked numerically that a random matrix whose antidiagonal elements are linked with a deterministic phase relation displays the same singular values distribution as a Hankel random matrix, provided that all its elements have zero mean and the same variance. The singular values distribution of a random Hankel matrix converges to a universal distribution $\rho_H(\lambda)$ of unbounded support [14]. To our knowledge, no analytical expression of ρ_H has been found and only a numerical simulation can provide an estimate for ρ_H, which has been done in Fig. 3(b) for comparison with the experimental data. The agreement between both curves is excellent.

Discriminating between multiple and single scattering can be done with optical correlation techniques [15]. Here, we propose to separate single and multiple-scattering contributions based on matrix properties. Let us write $\mathbf{K}$ as a sum of single and multiple-scattering contributions: $\mathbf{K} = \mathbf{K^S} + \mathbf{K^M}$. A change of coordinates $(x_i, x_j) \rightarrow (y_u, y_v)$ with $y_u = (x_i - x_j)/\sqrt{2}$, $y_v = (x_i + x_j)/\sqrt{2}$, amounts to rotating $\mathbf{K}$ by 45°. This yields a new matrix $\mathbf{A} = \mathbf{A^S} + \mathbf{A^M}$, for which the coherence of single-scattering signals now appears along the columns of $\mathbf{A^S}$. Ideally, we would like to get rid of $\mathbf{A^M}$. The characteristic space of single scattering is generated by the column vector $\mathbf{S}$ whose components are $s_u = \exp[jky_u^2/2R]$. Therefore a *filtered* matrix $\mathbf{A^F}$ can be obtained by projection: $\mathbf{A^F} = \mathbf{SS}^\dagger\mathbf{A}$. Its components read

$$a^F_{uv} = \frac{\exp(j2kR)}{R} \exp\left[jk\frac{y_u^2}{2R}\right]\Pi_v + s_u \sum_{u'=1}^{L} s^*_{u'} a^M_{u'v}, \quad (6)$$

where $\Pi_v = \sum_{d=1}^{N_d} A_d \exp[jk(y_v - X_d)^2/2R]$. In matrix notation, Eq. (6) reads $\mathbf{A^F} = \mathbf{A^S} + \mathbf{SS}^\dagger\mathbf{A^M}$. If multiple-scattering signals were strictly orthogonal to $\mathbf{S}$, the remaining term $\mathbf{SS}^\dagger\mathbf{A^M}$ would be zero. The final step is to go back to the original system of coordinates. This yields a filtered matrix $\mathbf{K^F}$, ideally devoid of multiple scattering, which is a promising perspective for imaging and detection.

As an experimental test, we now place a target (a hollow steel cylinder with diameter 15 mm) behind the forest of rods. In such condition, classical imaging (focusing a beam at the target depth z, in emission and reception, as would a lens with focal distance z [16]) completely fails (Fig. 5): the wave is not at all focused at the target position. This goes beyond simple aberration effects that, contrary to

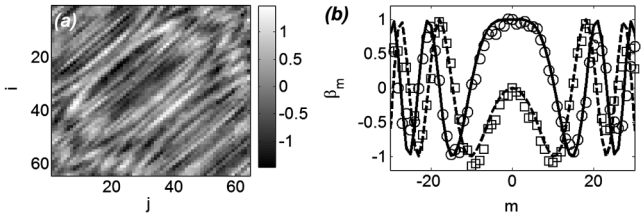

FIG. 4. Experimental results in a single-scattering sample (agar gel). (a) Real part of the matrix $\tilde{\mathbf{K}}(t, f)$ obtained at time $t = 184$ μs and frequency $f = 3.1$ MHz. (b) Real (white disks) and imaginary (white squares) parts of β_m are shown as a function of m and are compared to the real (solid line) and imaginary (dashed line) parts of Eq. (5).

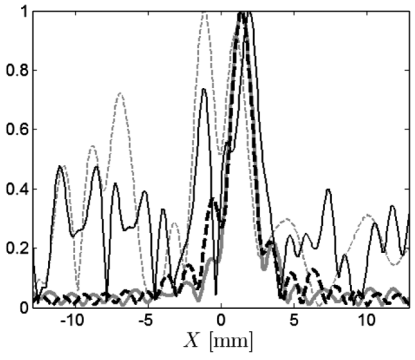

FIG. 5. Experimental results at the arrival time $t = 2L/c$ and frequency $f = 2.7$ MHz. Images are obtained with DORT applied to $\mathbf{K^F}$ (dashed black line), DORT applied to $\mathbf{K}$ (dashed gray line), classical focusing (solid black line). The ideal image is obtained without the multiple-scattering slab (gray solid line). Each image has been normalized by its maximum.

multiple scattering, could be compensated for by an adaptive lens. Here, given the slab thickness ($L = 20$ mm) the intensity of the coherent wave reflected by the target is divided by ~ 180 as it traverses twice the scattering slab, so multiple scattering dominates.

DORT (the French acronym for decomposition of the time-reversal operator) is another classical imaging technique [17]. The basic idea is the following: under the single-scattering approximation and for pointlike scatterers, each scatterer is essentially associated to one significant singular vector, corresponding to a nonzero singular value of $\mathbf{K}$. Physically, each singular vector of $\mathbf{K}$ corresponds to the wave front that, if it was sent from the array, would focus onto the corresponding scatterer. Therefore, by numerically backpropagating the singular vector in the supposedly homogeneous medium, an image of the corresponding target can be obtained. However, the one-to-one correspondence between scatterers and the λ_i is valid only in simple media in which scatterers are well separated, not too numerous, as long as the single-scattering assumption holds, which is clearly not the case here: DORT fails (see Fig. 5), as well as classical focusing.

Yet if we now apply the ''single-scattering filter'' before imaging with DORT, the target is successfully detected. The comparison with the ideal image (Fig. 5) that is obtained with the same array in water indicates that the ideal spatial resolution is nearly recovered, as if the multiple-scattering slab had been removed. It should be noticed though that the filter is not perfect: since each column of $\mathbf{A}$ contains a finite number $M \sim N/4$ of independent coefficients, multiple scattering is not totally suppressed, but its typical amplitude is reduced by $\sqrt{M}$.

This preliminary result is an illustration of potential applications of RMT to imaging in complex media with smart antennas, which we are currently working on. The agreement found between RMT and the experimental distribution $\hat{\rho}(\lambda)$ is not only of fundamental interest. In view of applications, it is important to have a reliable model for the distribution of singular values in the single or multiple-scattering regimes, e.g., in order to quantify the performance of such imaging methods.

The authors wish to thank J. Garnier, A. Tourin, C. Prada, J. de Rosny, and M. Fink for fruitful discussions, as well as anonymous reviewers and IMCODE(GDR CNRS 2253).

[1] P. Sheng, *Wave Scattering, Localization and Mesoscopic Phenomena* (Academic Press, New York, 1995); P. Sebbah, *Waves and Imaging Through Complex Media* (Kluwer Academic Publishers, Dordrecht, 2001).
[2] M. Mehta, *Random Matrices* (Academic Press, Boston, 1991).
[3] A. Tulino and S. Verdù, Found. Trends Commun. Inf. Theory **1**, 1 (2004).
[4] R. Sprik, A. Tourin, J. de Rosny, and M. Fink, Phys. Rev. B **78**, 012202 (2008).
[5] J. B. Pendry, A. Mac Kinnon, and P. J. Roberts, Proc. R. Soc. A **437**, 67 (1992).
[6] I. M. Vellekoop and A. P. Mosk, Phys. Rev. Lett. **101**, 120601 (2008).
[7] The quarter-circle law applies for singular values of a random matrix with zero-mean i.i.d elements, whatever their probability density function. It differs from the semi-circle law which applies for eigenvalues of a GOE or GUE matrix.
[8] A. Derode, V. Mamou, and A. Tourin, Phys. Rev. E **74**, 036606 (2006).
[9] V. Marčenko and L. Pastur, Math. USSR-Sbornik **1**, 457 (1967).
[10] Y. Kuga and A. Ishimaru, J. Opt. Soc. Am. A **1**, 831 (1984); E. Akkermans, P.-E. Wolf, R. Maynard, and G. Maret, J. Phys. (Les Ulis, Fr.) **49**, 77 (1988); A. Tourin, A. Derode, P. Roux, B. A. van Tiggelen, and M. Fink, Phys. Rev. Lett. **79**, 3637 (1997).
[11] J. H. Page, H. P. Schriemer, A. E. Bailey, and D. A. Weitz, Phys. Rev. E **52**, 3106 (1995).
[12] J. Goodman, *Statistical Optics* (Wiley & Sons, New York, 1985), Chap. 5.
[13] A. M. Sengupta and P. P. Mitra, Phys. Rev. E **60**, 3389 (1999).
[14] W. Bryc, A. Dembo, and T. Jiang, Annals Probability **34**, 1 (2006).
[15] W. V. Meyer, D. S. Cannell, A. E. Smart, T. W. Taylor, and P. Tin, Appl. Opt. **36**, 7551 (1997).
[16] B. Angelsen, *Ultrasound Imaging. Waves, Signals and Signal Processing* (Emantec, Trondheim, Norway, 2000).
[17] C. Prada and M. Fink, Wave Motion **20**, 151 (1994).